Article

In situ Formation of Multifunctional DNA Nanospheres for Sensitive and Accurate Dual-Mode Biosensor with Photoelectrochemical and Elecreochemical Assay

Hanmei Deng, Yaqin Chai, Ruo Yuan, and Yali Yuan

Anal. Chem., **Just Accepted Manuscript** • DOI: 10.1021/acs.analchem.0c00918 • Publication Date (Web): 13 May 2020

In situ Formation of Multifunctional DNA Nanospheres for Sensitive and Accurate Dual-Mode Biosensor with Photoelectrochemical and Elecreochemical Assay

Hanmei Deng, Yaqin Chai, Ruo Yuan, Yali Yuan*

Chongqing Engineering Laboratory of Nanomaterials & Sensor Technologies, College of Chemistry and Chemical Engineering, Southwest University, Chongqing 400715

* Corresponding author. Tel.: +86-23-68252277; Fax: +86-23-68253172.
E-mail address: y198688@swu.edu.cn (Y. L. Yuan)

For TOC Only

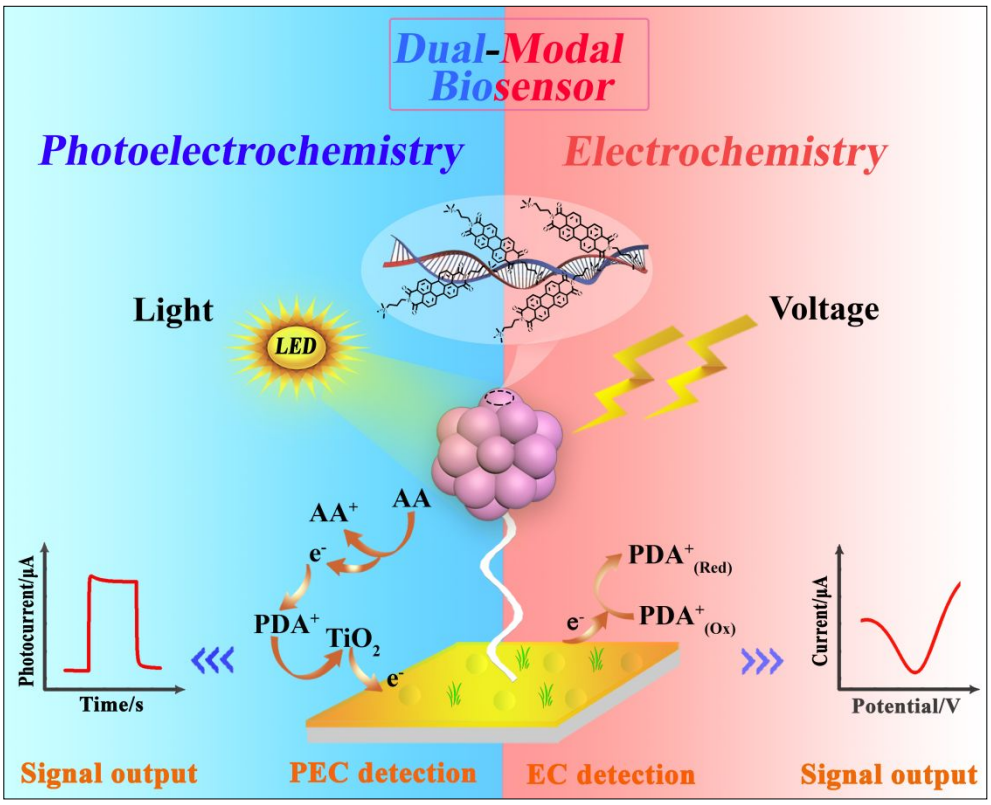
Dual-Modal Biosensor
Photoelectrochemistry
Electrochemistry
Light
LED
Voltage
AA+
AA
e-
PDA+
TiO2
e-
PDA+(Red)
e-
PDA+(Ox)
Photocurrent/μA
Time/s
Current/μA
Potential/V
Signal output
PEC detection
EC detection
Signal output

ABSTRACT

Herein, a photoelectrochemical (PEC) and electrochemical (EC) dual-mode biosensor with cationic N,N-bis(2-(trimethylammoniumiodide)propylene)perylene-3,4,9,10-tetracarboxyldiimide (PDA^+) decorected multifunctional DNA spheres in situ generated on electrode was proposed for sensitive and accurate detection of miRNA-141. By employing target-related ternary "Y" structure cleavage cycling reaction, the target DNA was converted into massive output DNA for being anchored on TiO_2 substrate, and hence triggering the rolling circle amplification (RCA) reaction. Upon the magnesium ions and PDA^+, the long DNA tails of RCA product were condensed to in situ form multifunctional DNA spheres. Notably, the distance between DNA spheres and TiO_2 substrate was short, thus forming an effective PDA^+-TiO_2 sensitization structure with fast electron transfer for acquiring an extremly enhanced PEC signal in the assistant of ascorbic acid (AA). Meanwhile, the cationic PDA^+ with large plane π-π skeleton enabled the possession of favorable redox-activity and substantial loading on DNA spheres, directly producing an obviously well-defined cathodic peak for implement of EC bio-detection on the same sensing platform. This approch not only avoided fussy aseembly of diverse signal indicators, but also significantly improved the sensitivity by utilizing cleavage cycling amplification and RCA strategies. Moreover, the distinct dual-response signals from two different transduction mechanisms and independent signal transduction could give a mutual supporting for accuracy improvement. As a reslut, a detection range of 0.1 fM to 1nM for PEC and 2 fM to 500 pM for EC were obtained for miRNA-141, providing a universal and efficient biosensing method with promising application in bioanalysis and early disease diagnosis.

KEYWORDS: dual-mode biosensor; PDA^+; multifunctional DNA spheres; distinct dual-response signals; two different transduction mechanisms

INTRODUCTION

Sensitive and accurate bio-detection has become one of the major and imperative researches in the fields of disease diagnosis, environmental monitoring and biological analysis.[1-4] Accordingly, enormous enthusiasm and attention have been foucus on exploiting various amplifing strategies by using different detection techniques, such as electrochemiluminescence (ECL),[5-7] elctrochemistry (EC),[8-10] colorimetry (CL),[11-13] photoelectrochemistry (PEC)[14-18] and fluorescence (FL).[19] Althrough acieved the superior sensitivity, most of the reported works for quantitative determination relied heavily on single-modal readout, which might suffer from the drawbacks of poor external anti-interference ability, high background and false signals caused by different operating personnel, nonstandard test process, or diverse experimental environments, thus influencing the accuracy of analysis to a certain extent.[20,21]

To be resolved, recently appeared the dual-modal bio-detection, in which the inter-verifiable dual-response derives from two different mechanisms and relatively independent signal transduction, such as PEC-CL,[22] PEC-EC,[23] ECL-FL.[24] Benefiting from the dissimilar transduction pattern, there is no interference between these two signaling routes in the dual-response analysis. Indeed, the adoping of diverse signal indicators is the direct way for dual-modal implementation. Nevertheless, the fussy indicator assembly operation, such as deposition[25,26] and hemin treatment[27] restrains its wide application. Comparatively, single indicator with exciting multifuction displays desirable superiority in dual-mode, which can not only simplify operation, but also reduce the uncontrollable variability in separated paths and different batches. Considering the simultaneous action of multiple roles by single indicator, however, most of the reported works restricted in depressed detection sensitivity or absolute change of detection batch.[28,29] Therefore, researching desirable signal

indicator for achiving the accurate, sensitive and convenient bio-detection is still a goal to pursue.

The cationic N,N-bis(2-(trimethylammoniumiodide)-propylene)perylene-3,4,9,10-tetracarbo -xyldiimide (PDA^+) is noticed as a kind of π-conjugated perylene derivative molecule with promising applications in electronics and optoelectronics. PDA^+ possesses high photon-to-electron conversion efficiency and narrower band gap, which is beneficial to sensitize wide-band materials for forming excellent sensitization structure, thereby acquiring a significantly enhanced PEC singal. Furthermore, the large plane π-π skeleton endows the PDA^+ with favorable redox-activity, providing an obviously well-defined cathodic peak for EC bio-detection. The PDA^+ thus becomes a good choice to act as bifunctional signal indicator for simply constructing PEC-EC dual-mode biosensor in accurate analysis. Besides that, the PDA^+ with positive charge at both sides of electron-deficient perylene core can not only realize the fuction as efficient DNA intercalator for nanoprobe formation, but also accommodate various DNA amplifying strategies for sensitivity improvement.

In this work, by coupling of target-related ternary "Y" structure cleavage cycling amplification, a novel multifunctional DNA nanospheres formed by PDA^+ intercalating in DNA long tails from rolling circle amplification (RCA) was in situ generated on TiO_2 substrate to construct PEC-EC dual-mode biosensor for accurate, sensitive and convenient detection of target miRNA-141. As depicted in Scheme 1, through cleavage cycling reaction, the target was converted into amounts of output DNA for being assembled on electrode. Afterwards, with the assistant of RCA and Mg^{2+}, the DNA nanospheres were thus in situ generated on electrode, which could load substantial PDA^+ signal indicators from dispersion solution to electrode surface and therefore effective reduced the distance between indicators and electrode, accelerating electron transport. PDA^+-carried multifunctional DNA nanospheres can in coordination with TiO_2 substrate to form PDA^+-TiO_2

sensitization structure, which availably promoted light-harvesting capability and effectively improved electron transfer to acquire enhanced photocurrent for sensitive PEC analysis. Additionally, PDA^+ with excellent electrochemical activity can produce an obvious electrochemical signal for complementary EC detection. the distinct dual-response signals from two different transduction mechanisms and independent signal transduction were applicable for dual-mode assay. This method utilized cleavage cycling amplification-triggered RCA reaction strategy to in situ generation of special condensed DNA spheres nanostructure with a good stability existed large number of repeat binding sites for internal encapsulation of PDA^+ as signal probes, hence the capacity to perform dual-mode assay using an indicator sensing platform was established for effective sensitivity and accuracy improvement. This innovative device offered a new perspective toward accurate bioassay and promising application in extensive analysis.

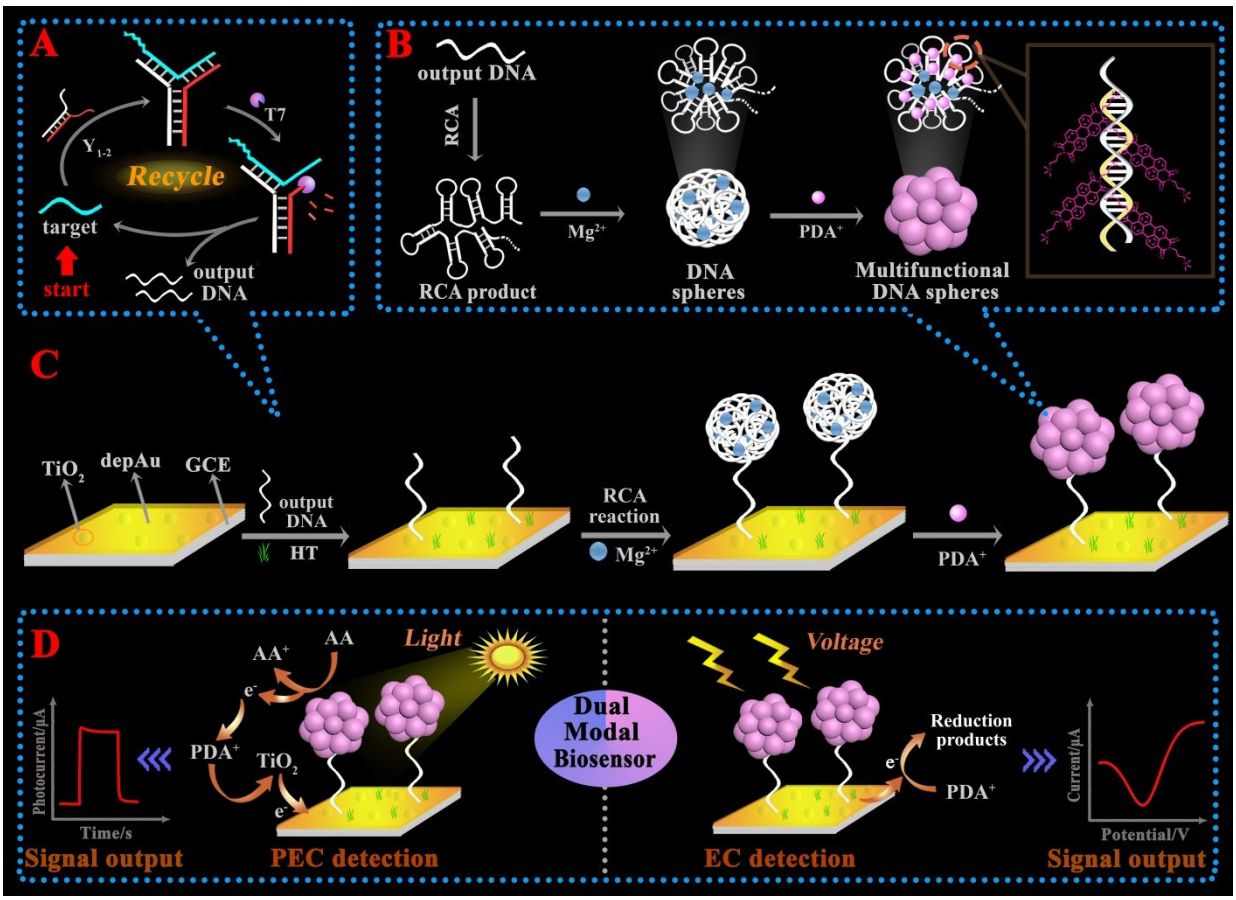

Scheme 1. Schematic illustration of (A) the target-induced recycle amplification with asistance of T7 endonuclease, (B) the process of forming multifunctional DNA spheres, (C) the fabrication of the biosensor, (D) PEC detection and EC detection by the dual-modal biosensor.

Experiment Section

Synthesis of PDA^+ compounds. Cationic PDA^+ was prepared by quaterisation (Scheme 2). Briefly, 0.50 g PTCDA and 1.5 mL DMAPA were mixed thoroughly, then 20.0 mL isobutanol solution was dispersed in above mixture, followed by violently stirring of 24 hours under 90℃ for the amidation reaction. Afterwards, the obtained crude product was washed with ethanol and further treated by 0.1 M NaOH solution at 80℃ for removing the unreacted raw materials. Immediately, 0.30 g above dried product and 0.15 mL CH_3I were transferred into toluene solution for 3 hours of reflux operation in nitrogen atmosphere. After washing with diethyl ether and vacuum drying, brown

red PDA^+ was finally collected for further use.

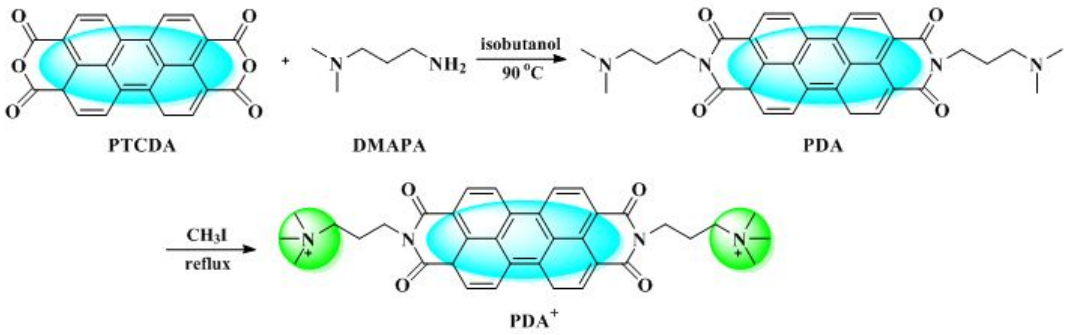

Scheme 2. Synthesis process of the PDA^+ compounds.

Fabrication of the biosensor decorated with multifunctional DNA nanospheres. First, 10 μL TiO_2 solution[30] was coated on pretreated glassy carbon electrode (GCE, Φ = 4 mm) and then dried in air, followed by immersing in $HAuCl_4$ solution for the deposition of Au nanoparticles (termed as depAu/TiO_2/GCE). Simultaneously, 50 μL mixture including 4 μM Y_1 and 4 μM Y_2 ssDNA was heated to 37°C for forming $Y_{1\text{-}2}$ structure. Afterward, 10 μL target miRNA-141 with different concentration was subjected to the $Y_{1\text{-}2}$ structure at 37°C and incubated for 2 h to generate the ternary Y junction. With the addition of 25 U T7 exonuclease, target-related cyclic amplification was triggered, leading to the conversion of a small amount of target into substantial output DNA. Subsequently, 10 μL obtained output DNA was attached on depAu/TiO_2/GCE and incubated overnight at 4°C. 5 μL 0.1 mM HT was then coated on electrode with incubation of 40 min for blocking residual binding site of depAu. Immediately, 5 μL 2 μM pretreated DNA with annealing operation and 2 μL 20 U T4 DNA ligase were attached on electrode and incubated overnight at 16°C for the intramolecular ligation. Next, 10 μL mixture containing 1U phi29 DNA polymerase and 2.5 mM dNTPs was incubated for 4 h at room temperature to initiate rolling circle amplification (RCA) reaction. $MgCl_2$ was then cultured to obtain Mg^{2+}-stabilized DNA nanoparticles at 30°C for 1 h.

After removing unbound reagents by washing at deionized water, resultant electrode was incubated with 5 μL 0.01 μM prepared PDA^+ for 2 h. Consequently, multifunctional DNA spheres were in situ generated by embedding positive charged PDA^+ into Mg^{2+}-stabilized DNA nanoparticles.

RESULT AND DISCUSSION

Morphology characterization of the nanomaterials. The morphology of different nanomaterials was characterized by SEM. TiO_2 nanoparticles displayed irregular spherical shape with a small diameter of about 40 nm (Figure 1A). Moreover, Mg^{2+}-stabilized DNA nanoparticles from RCA was evidently observed with a stable condensation of about 800 nm in diameter (Figure 1B). After embedding positive charged PDA^+ into Mg^{2+}-stabilized DNA nanoparticles (termed as multifunctional DNA spheres), numerous globular structure were clearly viewed (Figure 1C).

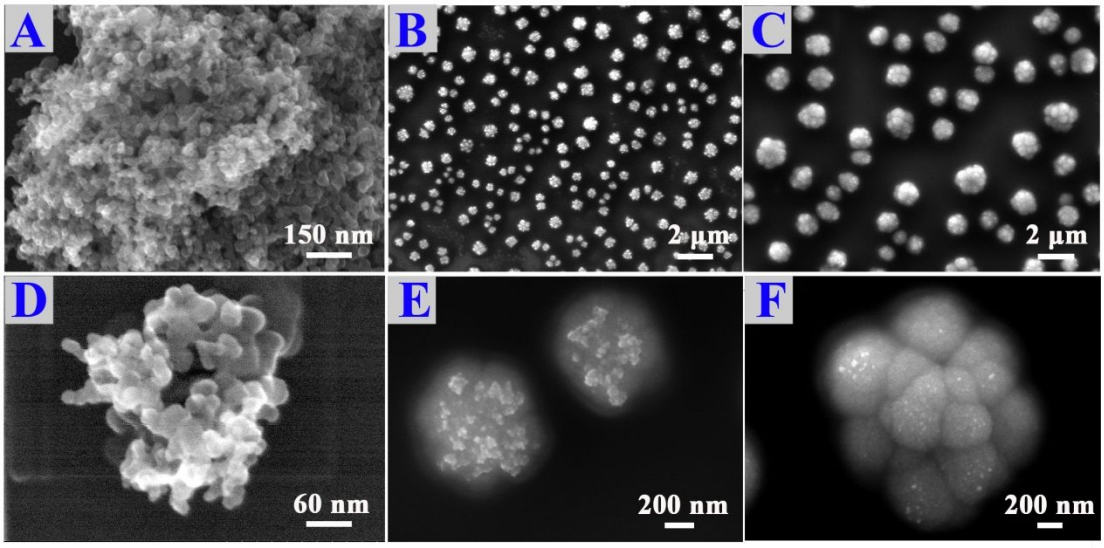

Figure 1. SEM images of (A) TiO_2 nanoparticles, (B) Mg^{2+}-stabilized DNA nanoparticles and (C) multifunctional DNA spheres, and corresponding magnification of (D) TiO_2 nanoparticles, (E) Mg^{2+}-stabilized DNA nanoparticles and (F) multifunctional DNA spheres.

Additionally, the formed multifunctional DNA spheres were bigger and fuller than Mg^{2+}-stabilized DNA nanoparticles, and even concavo-convex could be clearly viewed on the

surface. In order to have a clearer exhibition, the Figure 1D, Figure 1E and Figure 1F gave out the enlarged images of corresponding three nanomaterials mentioned above, respectively.

Characterization of the biosensor fabrication process and the generation mechanism of dual-response signals. To verify the fabrication process of biosensor, PEC measurements was conducted in 5 mL PBS containing 0.1 M electron donor AA, the photocurrent profiles toward stepwise-modified procedure were shown in Figure 2A. After coating TiO_2 nanoparticles on bare GCE, slightly enhanced photocurrent intensity was observed (curve b) compared to that of bare GCE (curve a), which is mainly due to the poor photoelectric activity of TiO_2 with wide energy band. When depAu was coated on TiO_2-modified electrode, the PEC signal further increased (curve c), the reason of which was that the depAu possessed the capability of accelerating electron transfer. However, with successively immobilizing output DNA (curve d) and HT (curve e) on electrode, decreased signals were appeared accordingly owing to their poor charge transfer performance. Remarkably, output DNA triggered the RCA reaction to form DNA nanospheres decorating with substantial positively charged PDA^+, thereby generating significantly enhanced photocurrent owing to excellent photoelectric activity of PDA^+ as sensitizer toward TiO_2 (curve f).

Meanwhile, EIS was carried out to further confirm the construction process of biosensor. As displayed in Figure 2B, bare GCE exhibited a small semicircle diameter (curve a) owing to the low electron transfer resistance (R_{et}). After the decoration of semiconductor TiO_2 nanoparticles on electrode, R_{et} value increased (curve b) in comparison with that of bare electrode. Afterwards, R_{et} value obviously decreased with coating of depAu, which on account of excellent conductivity of depAu nanoparticles (curve c). However, the R_{et} value constantly increased with the sequential assembly of negatively charged output DNA (curve d) and nonconductive HT (curve e). Once the

positive charged PDA^+ was incubated on modified electrode, a distinctly reduced R_{et} value was acquired (curve f) due to its superior electrochemical activity, thus indicating that the biosensor has been successful fabricated.

Moreover, to verify the feasibility of biosensor performed in a dual-mode, both the PEC and EC assay were employed. As shown in Figure 2C, in the absence of target, there were subtle initial signal produced by photoactive TiO_2-modified platform (red line). However, once the target miRNA-141 triggered the RCA reaction to generate multifunctional DNA nanospheres for further generation of PDA^+/TiO_2 sensitization structure, a dramatically increased photocurrent could be acquired (blue line). The photocurrent-generating mechanism was briefly described (Figure 2D). Significantly, formative integrating framework of DNA nanospheres-sensitized TiO_2 can availably promote light-harvesting capability and effectively depress electron-hole pair recombination for facilitating charge transfer. The PDA^+ with a narrower band gap of 2.14 eV is beneficial to well match wide-band TiO_2 (2.30 eV), thereby generating excellent sensitization structure. While being irradiated by light, the electron of PDA^+ transferred to the lowest unoccupied molecular orbital (LUMO) from the highest occupied molecular orbital (HOMO), thus migrating to the conduction band (CB) of TiO_2 and ultimately to the electrode via charge transfer adjustment mechanism. Simultaneously, AA as electron donor constantly captured the photogenerated holes (h^+) for inhibiting the recombination of the electron-hole pair, ensuring generation of stabilized and enhanced photocurrent signals. Meanwhile, as shown in Figure 2E, with non-existence of target, the electrochemical signals was negligible owing to non-electrochemical activity of TiO_2 (red line), which only acted as a platform for increasing surface area of electrode. Instead, PDA^+ with excellent electrochemical activity was immobilized depending on the present of target and then thus caused an

obvious electrochemical signal for quantitative target detection (blue line). The mechanism of producing electrochemical signal was illustrated as follows: PDA^+ with excellent electrochemical activity could transmute to reduce state from oxidation state under the action of electricity. Consequently, electrochemical signal was acquired. In sum, the proposed biosensor could be acted as dual-mode to implement photoelectrochmical and electrochemical detection with entirely different mechanisms.

Furthermore, the color changes about synthesis process of multifunctional DNA nanospheres were also investigated and were shown in Figure 2F, the solution containing substantial output ssDNA generated by target-induced cyclic amplification was transparent (left). However, after being treated with RCA reaction, output ssDNAs were converted into substantial DNA nanoparticles, thereby obtaining the turbid solution (middle). Afterwards, the decoration of PDA^+ on long DNA tails generated by RCA to form multifunctional DNA nanospheres, the color of solution was obviously changed into pink (right), which effectively displayed the formation process of multifunctional DNA nanospheres.

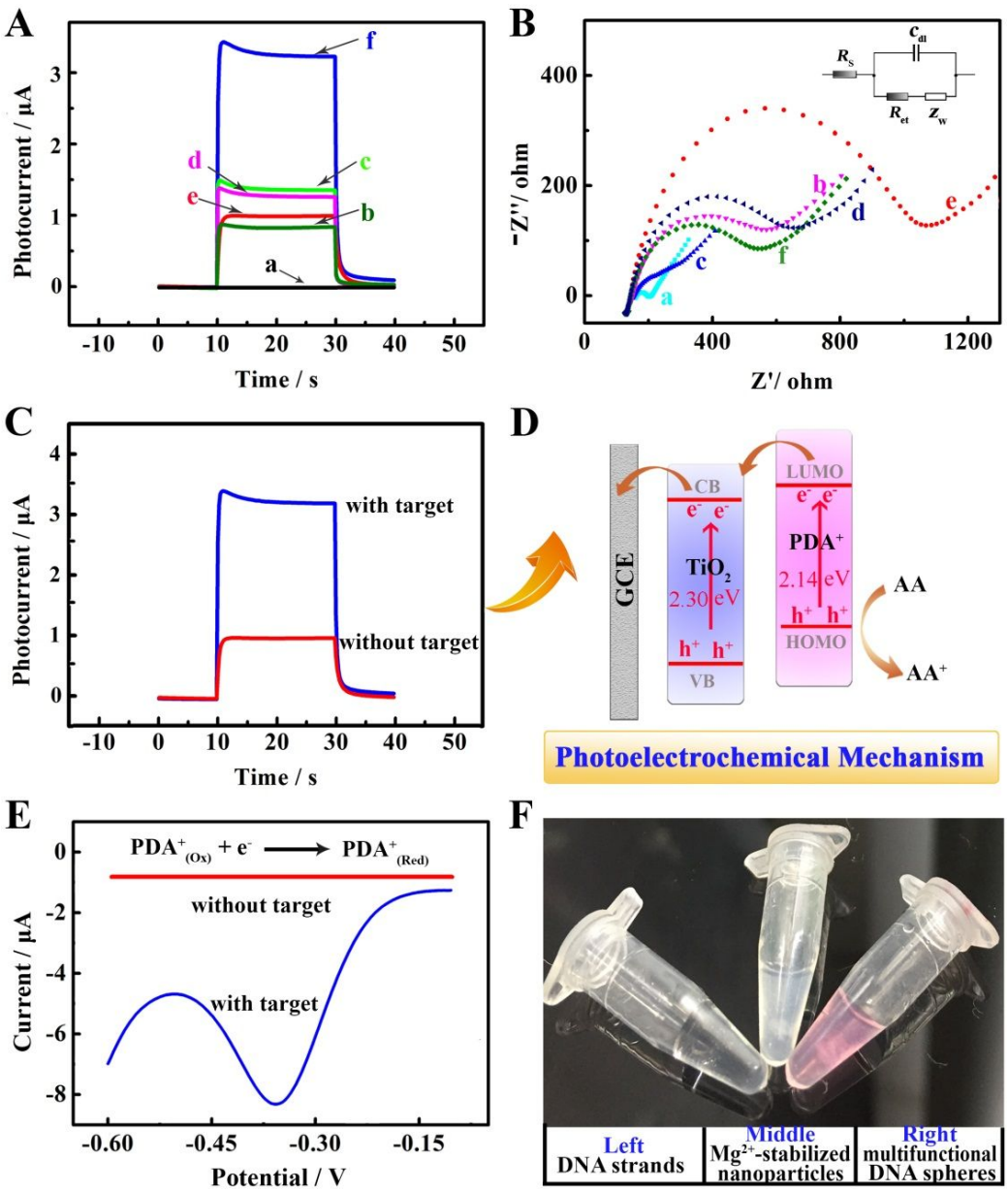

Figure 2. (A) PEC and (B) EIS characterization of the biosensor fabrication process: (a) bare GCE, (b) TiO_2/GCE, (c) depAu/TiO_2/GCE, (d) output DNA/depAu/TiO_2/GCE, (e) HT/output DNA/depAu/ TiO_2/GCE and (f) DNA nanosphere/HT/output DNA/depAu/TiO_2/GCE. (C) Photocurrent of the dual-mode biosensor in the absence and presence of target. (D) The detailed photocurrent-generating mechanism. (E) EC response of the dual-mode biosensor in the absence and presence of target (insert: the detailed mechanism for producing EC signal). (F) Photographs of DNA strands (left), Mg^{2+}-stabilized DNA nanoparticles from RCA (middle) and multifunctional DNA spheres embedded with PDA^+ (right).

Exploring sensitization effect of PDA^+ to substrate TiO_2 in PEC assay. To explore sensitization effect of PDA^+ toward TiO_2, the comparision of PEC responses using differecent modified electrodes was conducted under the identical condition. From Figure 3 we can see that the depAu/GCE (Figure 3A) and depAu/TiO_2/GCE (Figure 3B) have a photocurrent response of 0.02 μA and 0.83 μA, respectively. Furthermore, photocurrent response of multifunctional DNA nanospheres assembled depAu electrode (DNA nanospheres/depAu/GCE) was 0.75 μA (Figure 3C). Nevertheless, when multifunctional DNA nanospheres was assembled on depAu-coated TiO_2 substrate electrode (DNA nanospheres/depAu/TiO_2/GCE), photocurret response significantly increased to 3.25 μA (Figure 3D), response of which was about 3.9-fold and 4.3-fold higher than that of depAu/TiO_2/GCE and DNA nanospheres/depAu/GCE, attributing to that PDA^+ in DNA nanospheres could act as an outstanding sensitizer towards TiO_2. These results indicated that PDA^+-sensitized TiO_2 structure with high photoelectric properties was suitable to construct PEC biosensor for sensitive detection.

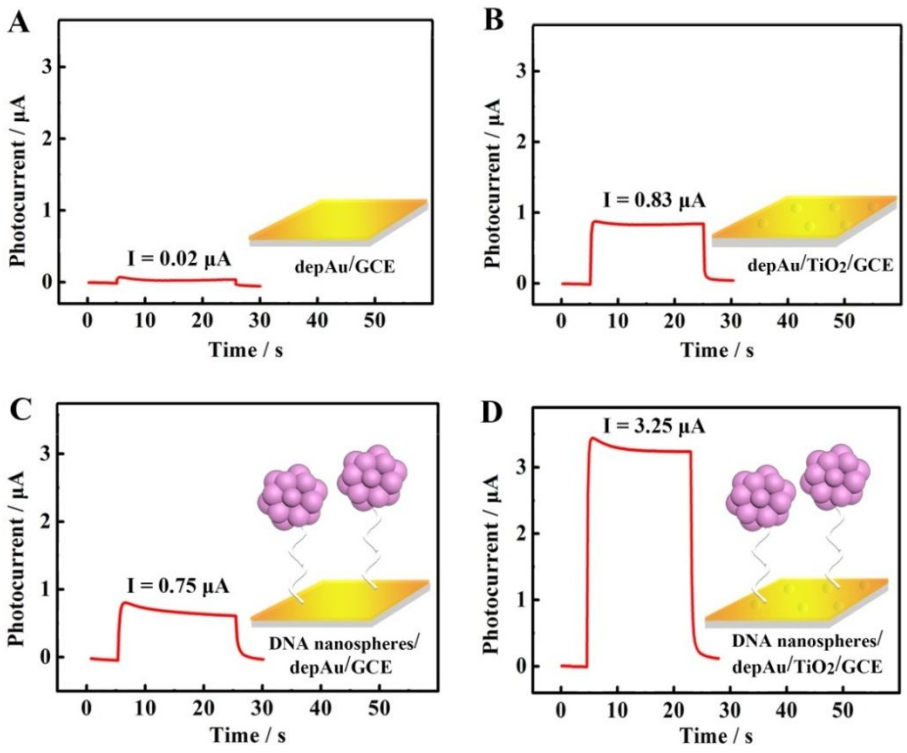

Figure 3. PEC responses of (A) depAu/GCE, (B) depAu/TiO_2/GCE, (C) DNA nanospheres/depAu/ GCE and (D)

DNA nanospheres/depAu/TiO_2/GCE in 0.1 M AA solution.

PEAG characterization of the target cycle-induced RCA reaction. Native PEAG measurement was executed to testify the practicability of target cycle-induced RCA reaction. As shown in Figure 4, target miRNA-141 and $Y_{1\text{-}2}$ junction in lane 1 and 2 displayed a distinct single band, respectively. Triplet-joint structure assembled from miRNA 141 and $Y_{1\text{-}2}$ junction migrated slower in the band of lane 3, which was attributed to its long oligonucleotide sequence. While the T7 endonuclease was added into sample containing triplet-joint structure, the band of which exhibited a faster movement (lane 4), sugguesting that output DNA with a small oligonucleotide sequence was generated at the assistant of T7 endonuclease. Nevertheless, in lane 5, where the output DNA was mixed with the auxiliaries for triggering RCA reaction, a bright band was noticed with extremely low mobility owing to generation of long DNA tails. The results of PAGE verfied the successful execution of target-induced RCA reaction in the presence of target miRNA-141.

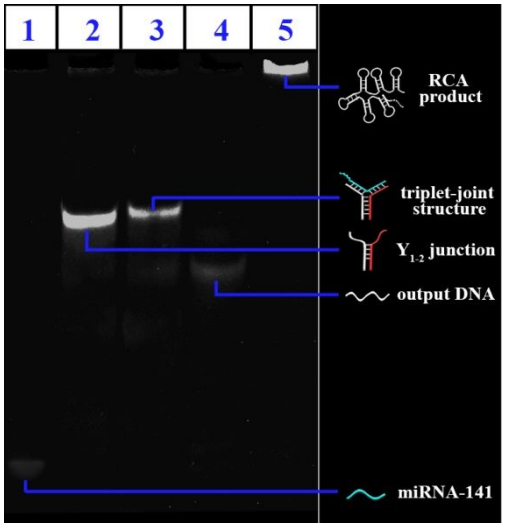

Figure 4. Native PEAG images: Lane 1, miRNA 141; lane 2, $Y_{1\text{-}2}$ junction; lane 3, triplet-joint structure; lane 4, output DNA; lane 5, RCA reaction product.

Analytical performance of dual-mode biosensor for miRNA-141 detection. To estimate the

anlytical perfamance of fabricated dual-mode PEC biosensor, PEC measurement was firstly implemented with various concentrations of miRNA-141. As illustrated in Figure 5A, PEC response raised gradually as the increase of miRNA concentration from 0.1 fM to 1nM. The calibration plot on the basis of photocurrent value was found to be linear in corresponding logarithm of miRNA-141 concentration (Figure 5B), and the linear equation was $I = 0.5521\ lgc + 4.429$ (where I and c were the photocurrent value and the concentration of miRNA-141, respectively). The limit of detection (LOD) was calculated to be 0.037 fM.

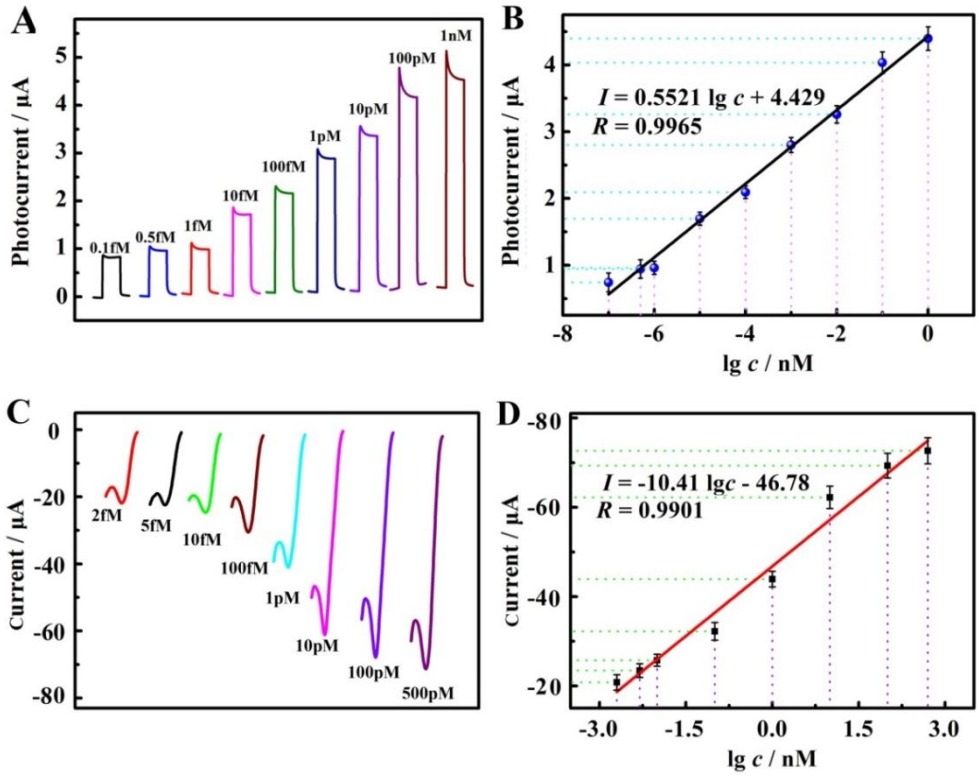

Figure 5. (A) PEC responses of the proposed biosensor with the incubation of various concentration of miRNA-141: 0.1 fM, 0.5 fM, 1 fM, 10 fM, 100 fM, 1 pM, 10 pM, 100 pM and 1nM. (B) The corresponding linear curve. (C) DPV responses of the proposed biosensor with the incubation of various concentration of miRNA-141: 2 fM, 5 fM, 10 fM, 100 fM, 1 pM, 10 pM, 100 pM and 500 pM. (D) The corresponding linear curve (error bar $n = 8$).

Simultaneously, electrochemical assay was also performed by recording DPV response. As shown in Figure 5C, with the increase of the miRNA-141 concentrations in the range from 2 fM to

500 pM, reduction peak also increased gradually. Moreover, the calibration plot displayed a good linear relationship between the reduction peak value and the logarithm of target concentrations. The calibration plot was I = -10.41 lgc + 46.78 (Figure 5D) with a detection limit of 0.67 fM ($3S_b/m$, where S_b is the standard deviation of the blank signals, m is the slope of calibration curve at lower concentration ranges). Additionally, comparison of the analytical performance among various test platforms was listed in table S4, which demonstrated that the proposed biosensor has an improved sensitivity and a wider linear due to the utilizing of target cycle-induced RCA reaction amplification.

Selectivity and stability of the fabricated biosensor. To investigate the selectivity of proposed biosensor, blank and diverse interfering substances including miRNA-151, miRNA-21, thrombin, DNA (a fragment of TP53 gene), and PSA were respectively incubated. Despite in the presence of 100 pM interference, no evident photocurrent response was monitored (Figure 6A). However, significant signal was observed at introducing of 1 pM target, which indicated a high selectivity of fabricated biosensor for the miRNA-141 assay. Furthermore, 1 pM miRNA-141 was incubated to investigate the stability of proposed biosensor under the periodic "off-on-off" light for 9 cycles. As depicted in Figure 6B, good stability was found with a relative standard deviation (RSD) of 0.98%.

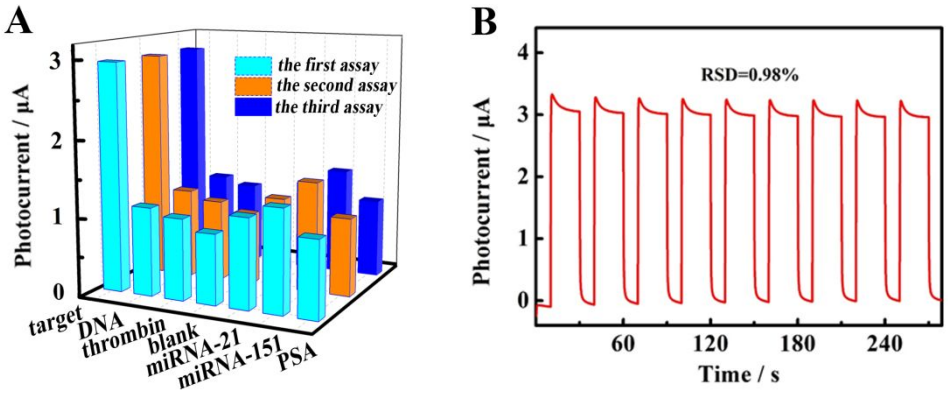

Figure 6. (A) Selectivity of the proposed PEC-EC biosensor towards miRNA-141 in comparison with the interference including miRNA-151, miRNA-21, thrombin, DNA and PSA. (B) Stability of the fabricated biosensor under the periodic "off-on-off" light for 9 cycles.

CONCLUSION

In summary, this work has developed a sensitive and accurate PEC-EC dual-mode biosensor based on the multifunctional DNA spheres as signal indicators. The massive output DNA from target-related ternary "Y" structure cleavage cycling reaction could trigger the RCA to in situ formation of PDA^+ decorected multifunctional DNA spheres on TiO_2 substrate. Since the DNA spheres were close to TiO_2 substrate, an effective PDA^+-TiO_2 sensitization structure and fast electron transfer could be acquired for generating extremly high PEC and EC signals. This approch ont only avoided fussy aseembly of diverse signal indicators, but also significantly improved the sensitivity by utilizing cleavage cycling amplification and RCA strategies, offering a new perspective for the future development of accurate, sensitive and convenient bioanalysis.

ACKNOWLEDGEMENTS

This work was supported by the Chongqing Research Program of Basic Research and Frontier Technology (cstc2018jcyjA0797), the Fundamental Research Funds for the Central Universities (XDJK2020TY002, XDJK2019B022, XDJK2018C041), and the National Natural Science Foundation (NNSF) of China (51473136, 21575116).

ASSOCIATED CONTENT

Supporting Information

Additional electronic information as pointed in the essay. This information is available free of charge via the Internet at http://pubs.acs.org

REFERENCES

(1) Zhao, X. J; Rovelyn, T. D.; Tan, W. H.; Ultrasensitive DNA Detection Using Highly Fluorescent

Bioconjugated Nanoparticles. *J. Am. Chem. Soc*. **2003**, *125*, 11474-11475.

(2) Xiao, M. S; Zou, K.; Li, L.; Wang, L. H.; Tian, Y.; Fan, C. H.; Pei, H. Stochastic DNA Walker in Droplets for Super-multiplex Bacteria Phenotype Detection. *Angew. Chem. Int. Ed*. **2019**, *131*, 15594-15600.

(3) Shi, X. M.; Wang, C. D.; Zhu, Y. C.; Zhao, W. W.; Yu, X. D.; Xu, J. J.; Chen, H. Y. 3D Semiconducting Polymer/graphene Networks: Toward Sensitive Photocathodic Enzymatic Bioanalysis. *Anal. Chem*. **2018**, *90*, 9687-9690.

(4) Li, J. Y.; Chen, R. K.; Zhang, Q. H.; Chen, J. N.; Gu, L.; Zhao, J.; Wang, Z. Y.; Dai, Z. H. Spectrum-quantified Morphological Evolution of Enzyme-protected Silver Nanotriangles by DNA-guided Postshaping. *J. Am. Chem. Soc.* **2019**, *141*, 19533-19537.

(5) Liu, G.; Jin, B. K.; Ma, C.; Chen, Z.; Zhu, J. J. Potential-resolved Electrochemiluminescence Nanoprobes for Visual Apoptosis Evaluation at Single-cell Level. *Anal. Chem*. **2019**, *91*, 6363-6370.

(6) Qi, H. L.; Zhang, C. X. Electrogenerated Chemiluminescence Biosensing. *Anal. Chem*. 2020, 92, 524-534.

(7) Yang, L.; Fan, D. W; Zhang, Y.; Ding, C. F.; Wu, D.; Wei, Q.; Ju, H. X. Ferritin-based Electrochemiluminescence Nanosurface Energy Transfer System for Procalcitonin Detection Using HWRGWVC Heptapeptide for Site-oriented Antibody Immobilization. *Anal. Chem*. **2019**, 91, 7145-7152.

(8) Li, L.; Zhang, Y.; Ge, S. G.; Zhang, L. N.; Cui, K.; Zhao, P. N.; Yu, J. H. Triggerable H_2O_2-cleavable Switch of Paper-based Biochips Endows Precision of Chemometer/ratiometric Electrochemical Quantification of Analyte in High-efficiency Point-of-care Testing. *Anal. Chem*. **2019**, *91*, 10273-10281.

(9) Zhang, T. T.; Xing, Y.; Song, Y.; Gu, Y.; Yan, X. Y.; Lu, N. N.; Liu，H.; Xu, Z. Q.; Zhang, Z. Q.; Yang, M. AuPt/MOF-Graphene: A Synergistic Catalyst with Surprisingly High Peroxidase-like Activity and its Application for H_2O_2 Detection. *Anal. Chem*. **2019**, *91*,

10589-10595.

(10) Yao, L. N.; Filice, Fraser P.; Yang, Q.; Ding, Z. F.; Su, B. Quantitative Assessment of Molecular Transport Through Sub‐3 nm Silica Nanochannels by Scanning Electrochemical Microscopy. *Anal. Chem*. **2019**, 91, *2*, 1548-1556.

(11) Li, S., Zhao, X. T.; Yu, X. X.; Wan, Y. Q.; Yin, M. Y.; Zhang, W. W.; Cao, B. Q.; Wang, H. Fe_3O_4 Nanozymes with Aptamer-Tuned Catalysis for Selective Colorimetric Analysis of ATP in Blood. *Anal. Chem*. **2019**, *91*, 14737-14742.

(12) Deng, H. H.; Lin, X. L.,; Liu, Y. H.; Li, K. L.; Zhuang, Q. Q.; Peng, H. P.; liu A. L.; Xia. X, H.; Chen, W. Chitosan-stabilized Platinum Nanoparticles as Effective Oxidase Mimics for Colorimetric Detection of Acid Phosphatase. *Nanoscale*, **2017**, *9*, 10292-10300.

(13) He, Y. F.; Li, X.; Xu, X. C.; Pan, J. M.; Niu, X. H. A Cobalt-based Polyoxometalate Nanozyme with High Peroxidase-mimicking Activity at Neutral pH for One-pot Colorimetric Analysis of Glucose. *J. Mater. Chem. B*. **2018**, *6*, 5750-5755.

(14) Lv, S. Z.; Zhang, K. Y.; Zeng, Y. Y.; Tang, D. P. Double Photosystems-based 'Z-scheme' Photoelectrochemical Sensing Mode for Ultrasensitive Detection of Disease Biomarker Accompanying Three-dimensional DNA Walker. *Anal. Chem*. **2018**, *90*, 7086-7093.

(15) Zhang, N.; Gao, H.; Xu, C. H.; Cheng, Y. X.; Chen, H. Y.; Xu, J. J. An Efficient Electrochemiluminescence Enhancement Strategy on Bipolar Electrode for Bioanalysis. *Anal. Chem*. **2019**, *91*, 12553-12559.

(16) Han, F. J.; Song, Z. Q.; Nawaz, M. H.; Dai, M. J.; Han, D. F.; Han, L. P.; Fan, Y. Y.; Xu, J. N.; Han, D. X.; Niu, L. MoS_2/ZnO-heterostructures-based Label-free, Visible-light-excited Photoelectrochemical Sensor for Sensitive and Selective Determination of Synthetic Antioxidant Propyl Gallate. *Anal. Chem*. **2019**, *91*, 10657-10662.

(17) Ge, L.; Hong, Q.; Li, H.; Li, F. A Laser-induced TiO_2-decorated Grapheme Photoelectrode for Sensitive Photoelectrochemical Biosensing. *Chem. Commun.* **2019**, *55*, 4945-4948.

(18) Hao, N.; Hua, R.; Chen, S. B.; Zhang, Y.; Zhou, Z.; Qian, J.; Liu, Q.; Wang, K. Multiple Signal-amplification via Ag and TiO_2 Decorated 3D Nitrogen Doped Graphene Hydrogel for Fabricating Sensitive Label-free Photoelectrochemical Thrombin Aptasensor. *Biosens. Bioelectron*. **2018**, *101*, 14-20.

(19) Hu, J.; Liu, M. H.; Zhang, C. Y. Construction of Tetrahedral DNA-quantum Dot Nanostructure with the Integration of Multistep Förster Resonance Energy Transfer for Multiplex Enzymes Assay. *ACS Nano*. **2019**, *13*, 7191-7201.

(20) Gao, X. S.; Li, H. K.; Zhao, Y.; Jie, G. F. Triple-helix Molecular Switch-based Versatile "off-on" Electrochemiluminescence and Fluorescence Bosensing Platform for Ultrasensitive Detection of Lipopolysaccharide by Multiple-amplification Strategy. *Biosens. Bioelectron*. **2019**, *143*, 111602.

(21) Lu, Y. W.; Zhao, H.; Fan, G. C.; Luo, X. L. Coupling Photoelectrochemical and Electrochemical Strategies in One Probe Electrode: Toward Sensitive and Reliable Dual-signal Bioassay for Uracil-DNA Glycosylase Activity. *Biosens. Bioelectron*. **2019**, *142*, 111569.

(22) Wei, J.; Chang, W. D. Qileng, A.; Liu, W. P.; Zhang, Y.; Rong, S. Y.; Lei, H. T.; Liu, Y. J. Dual-modal Split-type Immunosensor for Sensitive Detection of Microcystin-LR: Enzyme-induced Photoelectrochemistry and Colorimetry. *Anal. Chem*. **2018**, *90*, 9606-9613.

(23) Lu, Y. W.; Zhao, H.; Fan, G. C.; Luo, X. L. Coupling Photoelectrochemical and Electrochemical Strategies in One Probe Electrode: Toward Sensitive and Reliable Dual-signal Bioassay for Uracil-DNA Glycosylase Activity. *Biosens. Bioelectron*. **2019**, *142*, 111569.

(24) Xiaoshan Gao, Hongkun Li, Yu Zhao, Guifen Jie. Triple-helix Molecular Switch-based Versatile "off-on" Electrochemiluminescence and Fluorescence Biosensing Platform for Ultrasensitive Detection of Lipopolysaccharide by Multiple-amplification Strategy. *Biosens. Bioelectron*. **2019**, *143*, 111602.

(25) Wei, J.; Chang, W. D.; Qileng, A.; Liu, W. P.; Zhang, Y.; Rong, S. Y.; Lei, H. T.; Liu, Y. J.

Dual-modal Split-Type Immunosensor for Sensitive Detection of Microcystin-LR: Enzyme-induced Photoelectrochemistry and Colorimetry. *Anal. Chem*. **2018**, *90*, 9606-9613.

(26) Xue, S.; Li, Q.; Wang, L.; You, W.;Zhang, J.; Che, R. Copper-and Cobalt-codoped CeO_2 Nanospheres with Abundant Oxygen Vacancies as Highly Efficient Electrocatalysts for Dual-mode Electrochemical Sensing of MicroRNA. *Anal. Chem*. **2019**, *91*, 2659-2666.

(27) Mei, L. P.; Jiang, X. Y.; Yu, X. D.; Zhao, W. W.; Xu, J. J.; Chen, H. Y.. Cu Nanoclusters-encapsulated Liposomes: Toward Sensitive Liposomal Photoelectron-chemical Immunoassay. *Anal. Chem*. **2018**, *90*, 2749-2755.

(28) Xu, J. M; Zhang, Y. Li, L.; Kong, Q. K.; Zhang, L. N.; Ge, S. G.; Yu, J. H. Colorimetric and Electrochemiluminescence Dual-mode Sensing of Lead Ion Based on Integrated Lab-on-paper Device. *ACS Appl. Mater. Interfaces*. **2018**,*10*, 3431-3440.

(29) Nallal, M., Anantha Iyengar, G.; Pill-Lee, K. New Titanium Dioxide-based Heterojunction Nanohybrid for Highly Selective Photoelectrochemical–electrochemical Dual-mode Sensors. *ACS Appl. Mater. Interfaces*. **2017**, *9*, 37166-37183.

(30) Zhang, Y. H.; Li, M. J.; Wang, H. J.; Yuan, R.; Wei, S. P. Supersensitive Photoelectrochemical Aptasensor Based on Br, N, Codoped TiO_2 Sensitized by Quantum Dots. *Anal. Chem*. **2019**, *91*, 10864-10869.